Predicting the Bounds of Vehicle-Induced Bridge Responses Using the Interval Analysis Method

Qiling Zou[1]; Lu Deng, Ph.D., M.ASCE[2]; and Chao Jiang, Ph.D.[3]

Abstract: A method for predicting the bounds of vehicle-induced bridge responses with uncertain bridge and vehicle parameters is presented. The uncertainties in the parameters of the bridge and vehicle are represented with interval variables instead of conventional random variables with known probability distributions. First, a three-dimensional vehicle–bridge interaction (VBI) system, which has no closed-form solution and can account for road roughness, is established. Then, by introducing the interval analysis method (IAM) based on the first-order Taylor series expansion, the expressions of the bridge responses, including displacement and bending moment at the midspan, can be explicitly given as functions of the interval parameters, and the lower and upper bounds of the bridge responses are determined by the particle swarm algorithm instead of direct interval arithmetic to avoid excessive overestimation of the responses. The subinterval technique can also be adopted to improve the accuracy of the IAM. A numerical example is provided, and the results show that, compared with the conventional Monte Carlo method, the proposed IAM is capable of obtaining the bounds of the bridge deflection and bending moment without much sacrifice of accuracy while requiring much less computational effort. This indicates that the proposed method can be effectively and efficiently applied to predicting the bounds of the dynamic responses of complicated VBI systems with interval uncertainties. An example is also used to demonstrate the applicability of the IAM to field bridges when only limited information about the bridge and vehicle is available. **DOI: 10.1061/(ASCE)BE.1943-5592.0000911.**

Author keywords: Vehicle–bridge interaction; Uncertainty; Interval analysis; Taylor expansion; Dynamics.

Introduction

Vehicle-induced bridge responses have been extensively studied by many researchers. Among the numerical models developed to simulate the behavior of the vehicle–bridge interaction (VBI) system, deterministic parameters of vehicles and bridges are usually assumed, and the variation in parameters is usually considered by setting a series of predefined values within certain ranges, and deterministic analysis is then conducted with a combination of parameters with different values (Deng and Cai 2010; Ding et al. 2009; Huang et al. 1993; Liu et al. 2013). However, in real practice, both the bridge and vehicle are subject to various uncertainties that are usually difficult to predict. Therefore, such deterministic analysis with finite discrete values of parameters may not represent the nondeterministic characteristics of the parameters of the VBI system. Accurate prediction of vehicle-induced bridge responses requires reasonable consideration of these uncertainties.

There are three main approaches to modeling those uncertainties: probabilistic theory, fuzzy set, and interval analysis (Ma et al. 2013; Xia and Yu 2014). The probabilistic theory treats the uncertain parameters as random variables with known probability distributions, and has been widely applied to the study of VBI problems and other engineering problems (González et al. 2008; OBrien et al. 2010). Because of the requirement for obtaining sufficient statistical data to construct reliable probabilistic density functions of uncertain parameters, the probabilistic method may have poor performance in certain circumstances where valid data are sparse or lacking and the uncertain parameters are not random in nature (Ma et al. 2014; Sankararaman and Mahadevan 2011; Xia and Yu 2014).

The nonprobabilistic uncertainty, which results from the lack of knowledge and intrinsic drawbacks with the classical probabilistic methods, can be handled by two other approaches: the fuzzy set and interval analysis (Ma et al. 2013; Xia and Yu 2014). Xia and Yu (2014) pointed out that fuzzy analysis can be replaced by interval analysis using the α-level technique. Thus, interval analysis is the core method to model nonprobabilistic uncertainties. In interval analysis, the uncertain input parameters of the system are expressed as closed-bound intervals, and the goal of interval analysis is to obtain the bounds of the system responses through interval computations instead of Monte Carlo simulation, which requires excessive computational effort. Recent years have seen some applications of interval methods in engineering problems (Ma et al. 2013; Xia and Yu 2012; Zhang et al. 2010). The interval analysis method (IAM) was first introduced to the dynamic analysis of VBI systems by Liu et al. (2013). In their study, the simple VBI system consisted of a half-car model and a planar simply supported beam model, and the vehicle masses and the density, Young's modulus, and moment of inertia of the bridge were chosen as interval parameters. The lower and upper bounds of the bridge midspan deflection were obtained by the IAM. However, the application of their method to the study of VBI problems is limited in that their model is incapable of considering the VBI and the effect of road roughness. In fact, because of this limitation, the half-car model used in their study actually

[1]Graduate Student, College of Civil Engineering, Hunan Univ., Changsha, Hunan 410082, China. E-mail: zql0419@gmail.com

[2]Professor, Key Laboratory for Wind and Bridge Engineering of Hunan Province, College of Civil Engineering, Hunan Univ., Changsha, Hunan 410082, China (corresponding author). E-mail: denglu@hnu.edu.cn

[3]Professor, State Key Laboratory of Advanced Design and Manufacturing for Vehicle Body, College of Mechanical and Vehicle Engineering, Hunan Univ., Changsha, Hunan 410082, China. Email: jiangc@hnu.edu.cn

Note. This manuscript was submitted on August 26, 2015; approved on January 8, 2016; published online on February 29, 2016. Discussion period open until July 29, 2016; separate discussions must be submitted for individual papers. This paper is part of the ***Journal of Bridge Engineering***, © ASCE, ISSN 1084-0702.

degenerates into a couple of moving forces with constant magnitude.

This study presents an interval analysis method that can be used for the dynamic analysis of complex VBI systems with nonprobabilistic uncertainties. This method can deal with practical situations more accurately and efficiently than the traditional probabilistic methods when only limited information about the bridge and vehicle is available, and has the potential to provide a supplemental tool in bridge assessment.

The paper is organized as follows. First, a three-dimensional VBI model is established, and the equation of motion of the VBI model is introduced. Then, an IAM is developed to obtain the expressions of the bridge displacement and bending moment in the time domain based on the first-order Taylor series expansion, and the bounds of bridge responses are found by an optimization approach. Meanwhile, the subinterval technique is also adopted to improve the accuracy of the IAM. The dynamic analysis of a VBI system consisting of a bridge modeled by the grillage method and a 5-axle semitrailer truck under good-class road roughness conditions is used as an example for the illustration of this method. The Monte Carlo method (MCM) is also implemented to verify the effectiveness and efficiency of the proposed method, and the results obtained by two methods are compared and discussed. A field bridge example is also provided to illustrate the applicability of the IAM to practical problems when information about the bridge and vehicle parameters is limited.

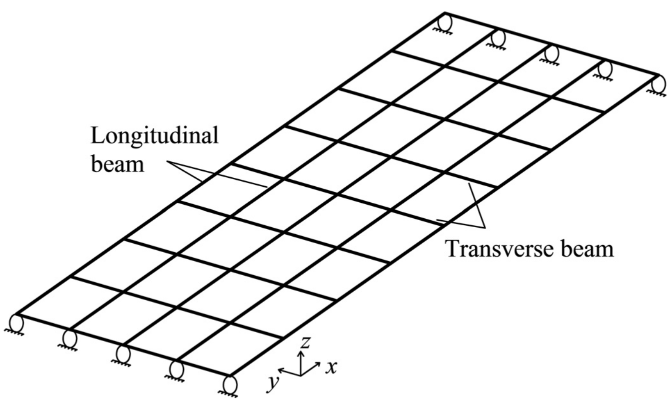

Fig. 1. Typical bridge modeled by the grillage method

VBI System

In the VBI system, the bridge model is created using the grillage method, by which the entire bridge is modeled by longitudinal and transverse Euler–Bernoulli beam elements. Each node of the space beam elements has six degrees of freedom (DOFs), including three translational and three rotational DOFs (Han et al. 2015). A typical simply supported multigirder bridge modeled by the grillage method is given in Fig. 1. It should be pointed out that the IAM presented here is not limited to grillage models only. The grillage

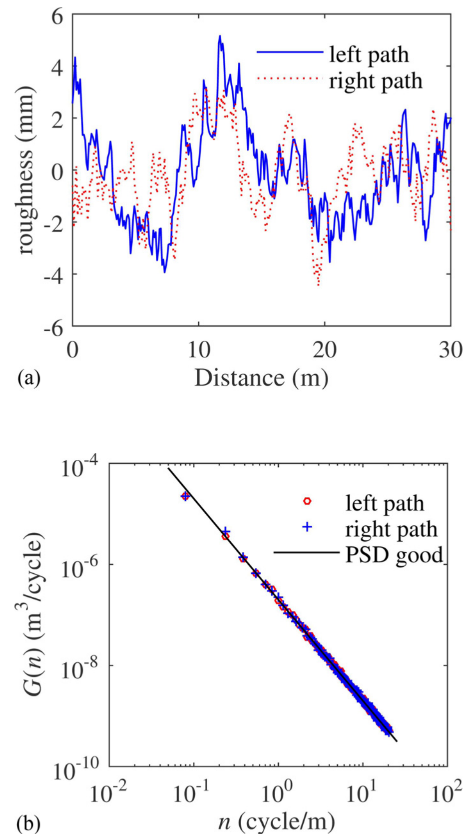

Fig. 3. Good-class parallel road roughness profiles: (a) roughness; (b) one-sided PSD

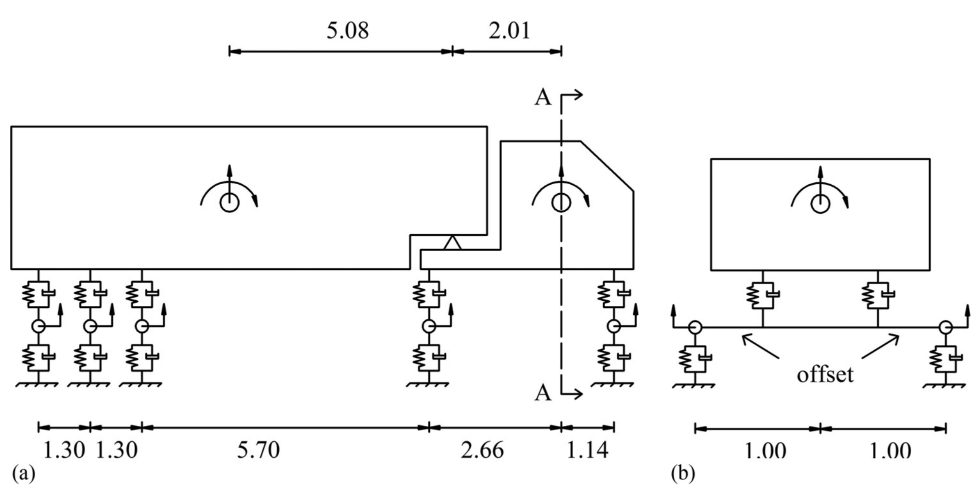

Fig. 2. Typical 5-axle vehicle model (meters) (adapted from OBrien et al. 2010): (a) side view; (b) Section A–A

model was adopted in this study to reduce the computational effort required by the MCM, which usually requires a large number of calculation times. To draw a fair comparison between the IAM and the MCM, the grillage model was therefore adopted here.

The vehicle is modeled with a three-dimensional spring–damper–mass system, where the vehicle bodies and axles are represented by rigid bodies with masses, and all components are connected by springs and dampers. This vehicle model can simulate the VBI more realistically while maintaining an acceptable level of complexity, and is widely used in most studies (Deng and Cai 2010; Huang et al. 1993; OBrien et al. 2010). Fig. 2 depicts a typical 5-axle semitrailer vehicle model used by OBrien et al. (2010).

The road surface roughness is generated as a zero-mean stationary Gaussian process based on a power spectral density (PSD) function (Dodds and Robson 1973). In this study, the correlation of the roughness profiles in the transverse direction was also taken into account based on the semianalytical coherency function proposed by Oliva et al. (2013). An example of two parallel good-class roughness profiles and their PSD us shown in Fig. 3.

Using the displacement relationship and the interaction force relationship at the contact points, the vehicle–bridge coupled system can be established by combining the equations of motion of both the bridge and vehicle, shown as follows:

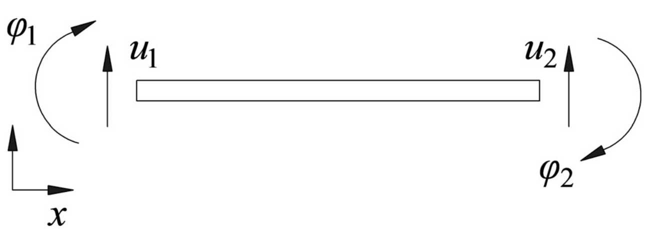

Fig. 4. DOFs of a beam in grillage model in the x–z plane

$$\begin{bmatrix} M_b & \\ & M_v \end{bmatrix}\begin{Bmatrix}\ddot{d}_b\\ \ddot{d}_v\end{Bmatrix} + \begin{bmatrix} C_b + C_{b-b} & C_{b-v} \\ C_{v-b} & C_v\end{bmatrix}\begin{Bmatrix}\dot{d}_b\\ \dot{d}_v\end{Bmatrix} + \begin{bmatrix} K_b+K_{b-b} & K_{b-v}\\ K_{v-b} & K_v\end{bmatrix}\begin{Bmatrix} d_b\\ d_v\end{Bmatrix} = \begin{Bmatrix}F_{b-r}\\ F_{v-r}+F_v^G\end{Bmatrix} \tag{1}$$

where the subscripts b, v, and r = bridge, vehicle, and road roughness, respectively; $\{d_b\}$, $\{\dot{d}_b\}$, and $\{\ddot{d}_b\}$ = displacement, velocity, and acceleration vectors of the bridge, respectively; $\{d_v\}$, $\{\dot{d}_v\}$, and $\{\ddot{d}_v\}$ = displacement, velocity, and acceleration vectors of the vehicle, respectively; $[M_b]$, $[C_b]$, and $[K_b]$ = mass, damping, and stiffness matrices of the bridge, respectively; $[M_v]$, $[C_v]$, and $[K_v]$ = mass, damping, and stiffness matrices of the vehicle, respectively; $\{F_vG\}$ = vector of gravity force of the vehicle; and C_{b-b}, C_{b-v}, C_{v-b}, K_{b-b}, K_{b-v}, K_{v-b}, F_{b-r}, and F_{v-r} are a result of the wheel–road contact forces.

When a vehicle moves across the bridge, the positions of the contact points as well as the values of the contact forces change, indicating that the damping and stiffness matrices and force vector of the VBI system in Eq. (1) are time-dependent and will change with the position of the vehicle on the bridge. These terms are calculated once the vehicle position on the bridge is determined and are updated at each time step. The equation of motion of the VBI system is solved in the time domain using the Newmark–β method. For more details about the equation of motion of the VBI system and its validation, readers can refer to Deng and Cai (2010).

IAM for the Dynamic Analysis of VBI System

Because bridge deflection and bending moment are two of the most important parameters that are widely used in bridge design and evaluation (Au et al. 2001; Deng et al. 2015), the IAM focuses on obtaining the lower and upper bounds of these two responses with the consideration of uncertainties inherent within the VBI system.

From Eq. (1), the general form of the equation of motion of the VBI system with interval parameters can be written as follows:

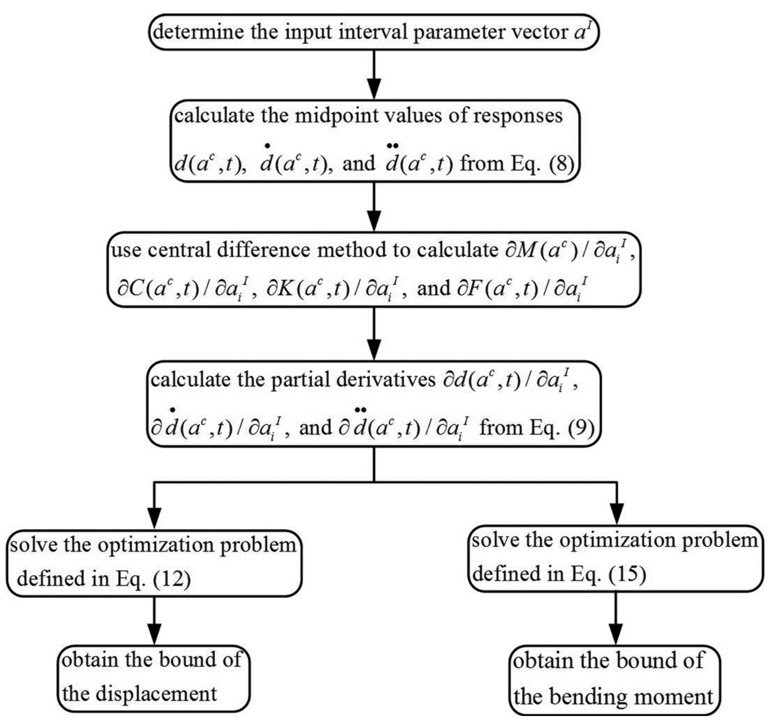

Fig. 5. Flowchart of IAM

$$M(a^I)\ddot{d}(a^I,t)+C(a^I,t)\dot{d}(a^I,t)+K(a^I,t)d(a^I,t)=F(a^I,t) \quad (2)$$

where $M(a^I)$, $C(a^I,t)$, $K(a^I,t)$, and $F(a^I,t)$ = interval mass, damping, stiffness matrices, and force vector, respectively; $d(a^I,t)$, $\dot{d}(a^I,t)$, and $\ddot{d}(a^I,t)$ = displacement, velocity, and acceleration interval vectors, respectively; and a^I = n-dimensional interval parameter vector belonging to an uncertain-but-bounded interval vector

$$a^I=[\underline{a},\overline{a}]=(a_i^I),\ a_i^I=[\underline{a_i},\overline{a_i}],\ i=1,2,\ldots,n \quad (3)$$

where $\underline{a}$ and $\overline{a}$ = lower and upper bounds of the interval parameter vector a, respectively; and $\underline{a_i}$ and $\overline{a_i}$ = lower and upper bounds of the interval parameter a_i, respectively.

The interval parameter a^I in Eq. (3) can also be expressed as

$$a^I=a^c+\Delta a^I=a^c+\Delta a\lambda \quad (4)$$

where

$$a^c=\frac{\underline{a}+\overline{a}}{2},\ \Delta a^I=[-\Delta a,\ \Delta a]=\Delta a\lambda,\ \lambda\in[-1,\ 1],\ \Delta a=\frac{\overline{a}-\underline{a}}{2} \quad (5)$$

where a^c, Δa, and Δa^I = midpoint value, interval width, and uncertain interval of the interval parameter a^I, respectively.

The uncertainty level of a_i^I is described as

$$\eta_i=\frac{\Delta a_i}{a_i^c} \quad (6)$$

Based on the first-order Taylor series expansion around the midpoint values of the interval parameters, the interval dynamic response of the system in Eq. (2) can be written as

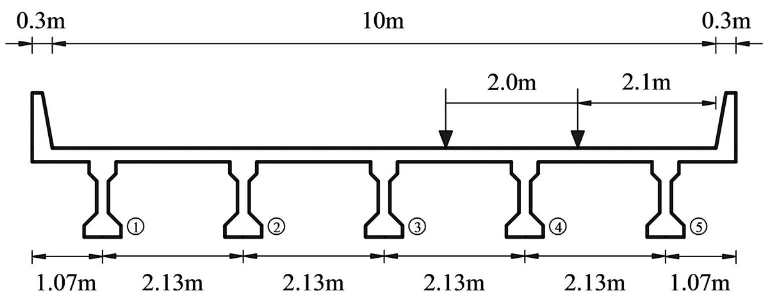

Fig. 6. Bridge cross section and loading case

Table 1. Interval Parameters of Bridge and Vehicle and Their Midpoint Values

Parameter	No.	Description of parameter	Midpoint value
Bridge parameter	a_1	Young's modulus of the girder (Pa)	3.450×10^{10}
	a_2	Young's modulus of the diaphragm and deck (Pa)	2.470×10^{10}
	a_3	Mass of exterior girder (N/m)	1.896×10^{4}
	a_4	Mass of interior girder (N/m)	1.431×10^{4}
	a_5	Mass of intermediate diaphragm (N/m)	3.029×10^{3}
	a_6	Mass of diaphragm at ends (N/m)	1.664×10^{3}
	a_7	Torsional moment of inertia of girder (m^4)	6.650×10^{-3}
	a_8	Torsional moment of inertia of intermediate diaphragm (m^4)	6.477×10^{-3}
	a_9	Torsional moment of inertia of diaphragm at ends (m^4)	2.876×10^{-3}
	a_{10}	Bending moment of inertia of girder (m^4)	4.012×10^{-2}
	a_{11}	Bending moment of inertia of intermediate diaphragm (m^4)	9.740×10^{-3}
	a_{12}	Bending moment of inertia of diaphragm at ends (m^4)	4.750×10^{-3}
Vehicle parameter	a_{13}	Tractor sprung mass (kg)	7×10^{3}
	a_{14}	Trailer sprung mass (kg)	3.877×10^{4}
	a_{15}	Pitch moment of inertia of tractor body (kg·m^2)	4.604×10^{3}
	a_{16}	Pitch moment of inertia of trailer body (kg·m^2)	1.630×10^{4}
	a_{17}	Tractor steer axle mass (kg)	7×10^{2}
	a_{18}	Tractor rear axle mass (kg)	1×10^{3}
	a_{19}	Trailer tridem axle mass (individual) (kg)	8×10^{2}
	a_{20}	Tractor steer suspension stiffness (N/m)	3×10^{5}
	a_{21}	Tractor rear suspension stiffness (N/m)	5×10^{5}
	a_{22}	Trailer tridem suspension stiffness (individual) (N/m)	4×10^{5}
	a_{23}	Tire stiffness (N/m)	7.500×10^{5}
	a_{24}	Suspension damping (N·s/m)	5×10^{3}
	a_{25}	Tire damping (N·s/m)	3×10^{3}
	a_{26}	Suspension offset of steer and trailer axles (m)	1×10^{-1}
	a_{27}	Suspension offset of rear axle (m)	5×10^{-1}

$$\ddot{d}(a^I,t) = \ddot{d}(a^c,t) + \sum_{i=1}^{n} \frac{\partial \ddot{d}(a^c,t)}{\partial a_i^I}(a_i^I - a_i^c)$$

$$\dot{d}(a^I,t) = \dot{d}(a^c,t) + \sum_{i=1}^{n} \frac{\partial \dot{d}(a^c,t)}{\partial a_i^I}(a_i^I - a_i^c)$$

$$d(a^I,t) = d(a^c,t) + \sum_{i=1}^{n} \frac{\partial d(a^c,t)}{\partial a_i^I}(a_i^I - a_i^c) \quad (7)$$

The midpoint responses $d(a^c,t)$, $\dot{d}(a^c,t)$, and $\ddot{d}(a^c,t)$ can be obtained directly by solving the following equation:

$$M(a^c)\ddot{d}(a^c,t) + C(a^c,t)\dot{d}(a^c,t) + K(a^c,t)d(a^c,t) = F(a^c,t) \quad (8)$$

whereas the partial derivative terms $\partial d(a^c,t)/\partial a_i^I$, $\partial \dot{d}(a^c,t)/\partial a_i^I$, and $\partial \ddot{d}(a^c,t)/\partial a_i^I$ can be obtained by the following sensitivity analysis.

Taking the first-order partial derivative of both sides of Eq. (2) with respect to the interval parameter a_i^I around its midpoint value gives the following:

$$M(a^c)\frac{\partial \ddot{d}(a^c,t)}{\partial a_i^I} + C(a^c,t)\frac{\partial \dot{d}(a^c,t)}{\partial a_i^I} + K(a^c,t)\frac{\partial d(a^c,t)}{\partial a_i^I}$$
$$= \frac{\partial F(a^c,t)}{\partial a_i^I} - \frac{\partial M(a^c)}{\partial a_i^I}\ddot{d}(a^c,t) - \frac{\partial C(a^c,t)}{\partial a_i^I}\dot{d}(a^c,t)$$
$$-\frac{\partial K(a^c,t)}{\partial a_i^I}\partial d(a^c,t) \quad i = 1,2,\ldots,n \quad (9)$$

The left sides of Eqs. (8) and (9) both have similar forms. The terms $\partial M(a^c)/\partial a_i^I$, $\partial C(a^c,t)/\partial a_i^I$, $\partial K(a^c,t)/\partial a_i^I$, and $\partial F(a^c,t)/\partial a_i^I$ on the right side of Eq. (9) can be computed by numerical differentiation methods, such as the central difference method, as follows:

$$\frac{\partial M(a^c)}{\partial a_i^I} = \frac{M(a^c + \delta a_i) - M(a^c - \delta a_i)}{2\delta a_i}$$
$$\frac{\partial C(a^c,t)}{\partial a_i^I} = \frac{C(a^c + \delta a_i,t) - C(a^c - \delta a_i,t)}{2\delta a_i}$$
$$\frac{\partial K(a^c,t)}{\partial a_i^I} = \frac{K(a^c + \delta a_i,t) - K(a^c - \delta a_i,t)}{2\delta a_i}$$
$$\frac{\partial F(a^c,t)}{\partial a_i^I} = \frac{F(a^c + \delta a_i,t) - F(a^c - \delta a_i,t)}{2\delta a_i} \quad i = 1,2,\ldots,n \quad (10)$$

where $\delta a_i \leq \Delta a_i$, δa_i = small variation of the ith parameter in the interval parameter vector a^I.

By substituting $d(a^c,t)$, $\dot{d}(a^c,t)$, and $\ddot{d}(a^c,t)$ from Eq. (8) and $\partial M(a^c)/\partial a_i^I$, $\partial C(a^c,t)/\partial a_i^I$, $\partial K(a^c,t)/\partial a_i^I$, and $\partial F(a^c,t)/\partial a_i^I$ from Eq. (10) into the right side of Eq. (9), Eq. (9) can also be solved by the Newmark–β method because it possesses the general form of the equation of motion, similar to Eq. (8). It should be noticed that $\partial C(a^c,t)/\partial a_i^I$, $\partial K(a^c,t)/\partial a_i^I$, and $\partial F(a^c,t)/\partial a_i^I$ are all time-dependent terms.

Once the system responses and their partial derivatives at the midpoint value of the interval parameters are obtained, according to Eq. (7), the lower and upper bounds of displacement response can be explicitly given as follows based on the interval arithmetic:

$$\underline{d(a^I,t)} = d(a^c,t) - \sum_{i=1}^{n}\left|\frac{\partial d(a^c,t)}{\partial a_i^I}\right|\Delta a_i$$
$$\overline{d(a^I,t)} = d(a^c,t) + \sum_{i=1}^{n}\left|\frac{\partial d(a^c,t)}{\partial a_i^I}\right|\Delta a_i \quad (11)$$

However, it should be noted that significant overestimation may be induced by the *wrapping effect* of the interval arithmetic in Eq. (11). To address this problem, global optimization algorithms, such as the particle swarm optimization (PSO), can be used to reduce the overestimation to a great extent and obtain tighter and more reasonable bounds (Wu et al. 2015). Therefore, the bounds of displacement can be calculated by the following optimization problem:

$$\min_{\lambda} \text{ or } \max_{\lambda} d(a^I,t) = d(a^c,t) + \sum_{i=1}^{n}\frac{\partial d(a^c,t)}{\partial a_i^I}\Delta a_i \lambda_i$$
$$\text{s.t.} \quad -1 \leq \lambda_i \leq 1, \; i = 1,2,\ldots,n \quad (12)$$

In addition, based on the FEM, the element internal forces resulting from structure deformation can be obtained by multiplying the element stiffness matrix by the displacement vector of the corresponding DOFs. Therefore, the bending moment at the end of the beam used in the grillage method, which correspond to four DOFs (u_1, φ_1, u_2, and φ_2) as shown in Fig. 4, can be expressed as

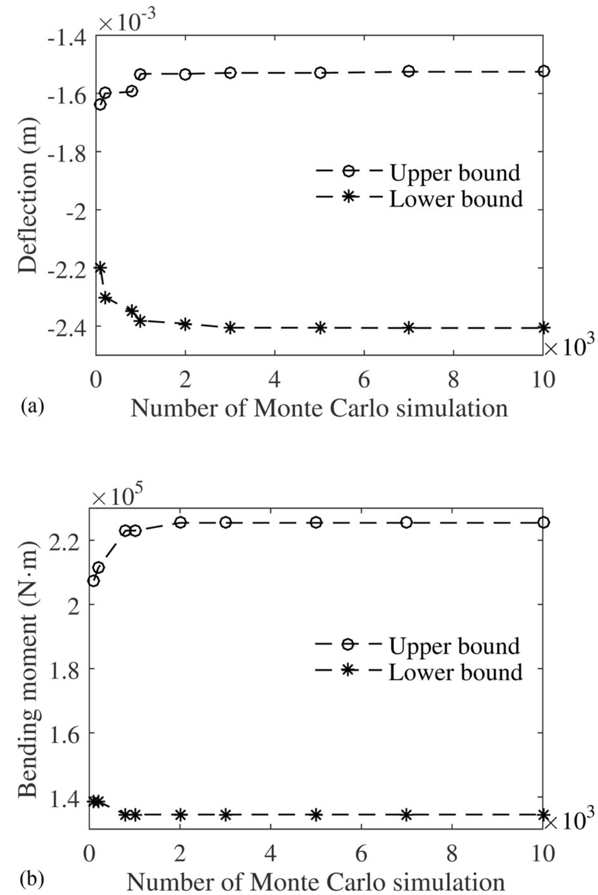

Fig. 7. Convergence test results of the MCM (η = 0.10): (a) deflection; (b) bending moment

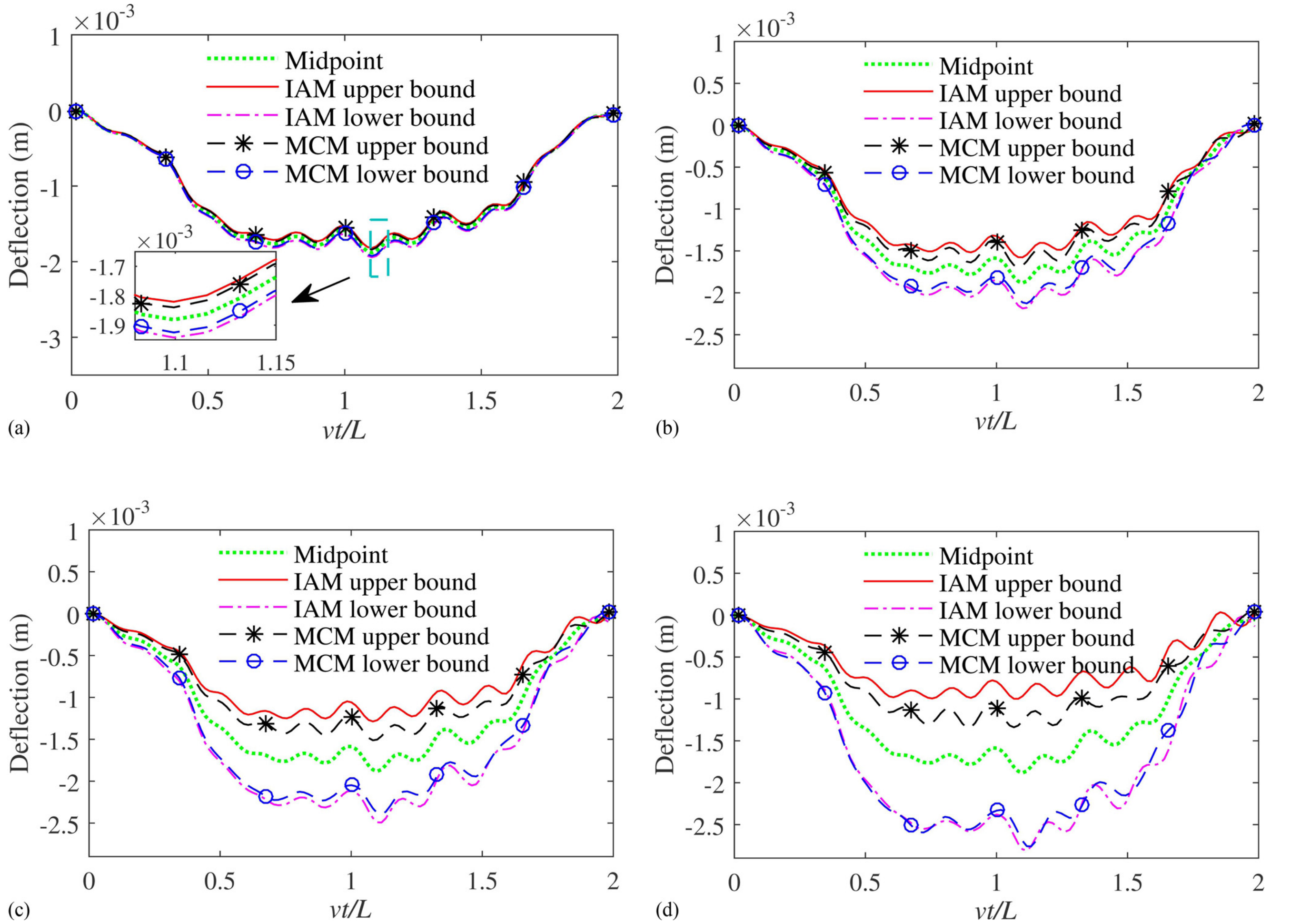

Fig. 8. Bounds of deflection time histories at the midspan of Girder 4 under different levels of uncertainty (vehicle speed = 20 m/s): (a) $\eta = 0.01$; (b) $\eta = 0.05$; (c) $\eta = 0.10$; (d) $\eta = 0.15$

$$m_1 = \left[-\frac{6EI_{yy}}{l^2} \quad \frac{4EI_{yy}}{l} \quad \frac{6EI_{yy}}{l^2} \quad \frac{2EI_{yy}}{l}\right]\begin{Bmatrix} u_1 \\ \varphi_1 \\ u_2 \\ \varphi_2 \end{Bmatrix}$$

$$= EI_{yy}\left(-\frac{6}{l^2}u_1 + \frac{4}{l}\varphi_1 + \frac{6}{l^2}u_2 + \frac{2}{l}\varphi_2\right) \qquad (13)$$

where E and I_{yy} = Young's modulus and second moment of inertia of the beam, respectively; and l = element length.

When E and I_{yy} are considered as interval parameters, which are denoted as $a_E I$ and $a_{I_{yy}} I$, respectively, substituting the Taylor series expansion of displacement in Eq. (7) into Eq. (13) yields

$$m_1(a^I, t) = (a_E^c + \Delta a_E^I)(a_{I_{yy}}^c + \Delta a_{I_{yy}}^I)\left(-\frac{6}{l^2}u_1(a^c, t) + \frac{4}{l}\varphi_1(a^c, t) + \frac{6}{l^2}u_2(a^c, t) + \frac{2}{l}\varphi_2(a^c, t) + \sum_{i=1}^{n}\left(-\frac{6}{l^2}\frac{\partial u_1(a^c, t)}{\partial_{a_i}^I} + \frac{4}{l}\frac{\partial \varphi_1(a^c, t)}{\partial_{a_i}^I} + \frac{6}{l^2}\frac{\partial u_2(a^c, t)}{\partial_{a_i}^I} + \frac{2}{l}\frac{\partial \varphi_2(a^c, t)}{\partial_{a_i}^I}\right)\Delta a_i^I\right) \qquad (14)$$

Unlike Eq. (7), where the bridge deflection is transformed into the linear combinations of those interval parameters, Eq. (14) involves the multiplication of several interval parameters; as a result, the lower and upper bounds of the bending moment are not easy to determine explicitly. Meanwhile, the partial derivatives of displacements are influenced by a_E^I and $a_{I_{yy}}^I$. These scenarios with multiple occurrences of some interval parameters in the same expression are called dependency phenomenon, which can further lead to an extreme overestimation in the direct interval arithmetic (Muhanna and Mullen 2001). Instead, global optimization algorithms are also adopted here to find the minimum and maximum of the bending moment. The equivalent optimization problem is defined as follows:

$$\min_{\lambda} \text{ or } \max_{\lambda} m_1(\lambda, t) = (a_E^c + \Delta a_E \lambda_E)(a_{I_{yy}}^c + \Delta a_{I_{yy}} \lambda_{I_{yy}})\left(-\frac{6}{l^2}u_1(a^c, t) + \frac{4}{l}\varphi_1(a^c, t) + \frac{6}{l^2}u_2(a^c, t) + \frac{2}{l}\varphi_2(a^c, t) + \sum_{i=1}^{n}\left(-\frac{6}{l^2}\frac{\partial u_1(a^c, t)}{\partial a_i^I} + \frac{4}{l}\frac{\partial \varphi_1(a^c, t)}{\partial a_i^I} + \frac{6}{l^2}\frac{\partial u_2(a^c, t)}{\partial a_i^I} + \frac{2}{l}\frac{\partial \varphi_2(a^c, t)}{\partial a_i^I}\right)\Delta a_i \lambda_i\right)$$

$$\text{s.t.} -1 \le \lambda_i \le 1, \; i = 1, 2, \ldots, n \qquad (15)$$

A flowchart of the IAM for finding the lower and upper bounds of the bridge displacement and bending moment in the VBI system is shown in Fig. 5.

Because of the use of the first-order Taylor expansion, the accuracy of the IAM is affected by the uncertainty levels of interval parameters. Large uncertainty levels may lead to unacceptable overestimation of the bounds of the target bridge responses. Therefore, the subinterval technique can be adopted to refine the results of the IAM when necessary (Xia and Yu 2014).

For the interval parameter a_i^I ($i = 1, 2, \ldots, n$), the original interval $2\Delta a_i$ can be further divided into a series of uniform subintervals, which can be defined as

$$a_{s_i}^I = \left[\underline{a}_i^I + 2(s-1)\Delta a_i/L_i, \underline{a}_i^I + 2s\Delta a_i/L_i\right], \quad s = 1, 2, \ldots, L_i \tag{16}$$

where L_i = number of subintervals of a_i^I; and $a_{s_i}^I$ = s_ith subinterval of the ith interval parameter a_i^I.

The uncertainty level of $a_{s_i}^I$ is obviously less than that of the original a_i^I, thus the accuracy of the IAM can be improved. Meanwhile, choosing one subinterval from each interval parameter results in a total of $L_1 \cdot L_2 \cdot, \ldots, \cdot L_n$ combinations of subintervals, which also means that the aforementioned interval analysis procedure needs to be carried out $L_1 \cdot L_2 \cdot, \ldots, \cdot L_n$ times, and the bounds yielded by each interval analysis should be merged through the interval union operation to yield the global bounds (Xia and Yu 2014). Apparently, more subintervals will lead to more accurate final bounds, while requiring more computational effort at the same time. Therefore, to achieve

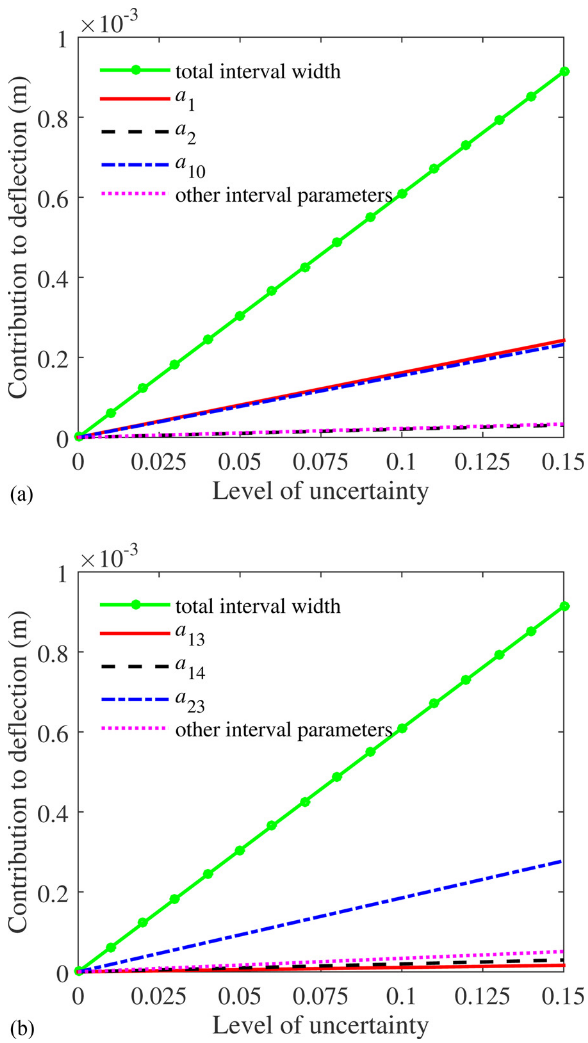

Fig. 9. Contribution of each interval parameter to the interval width of the maximum deflection (vehicle speed = 20 m/s): (a) bridge's parameters; (b) vehicle's parameters

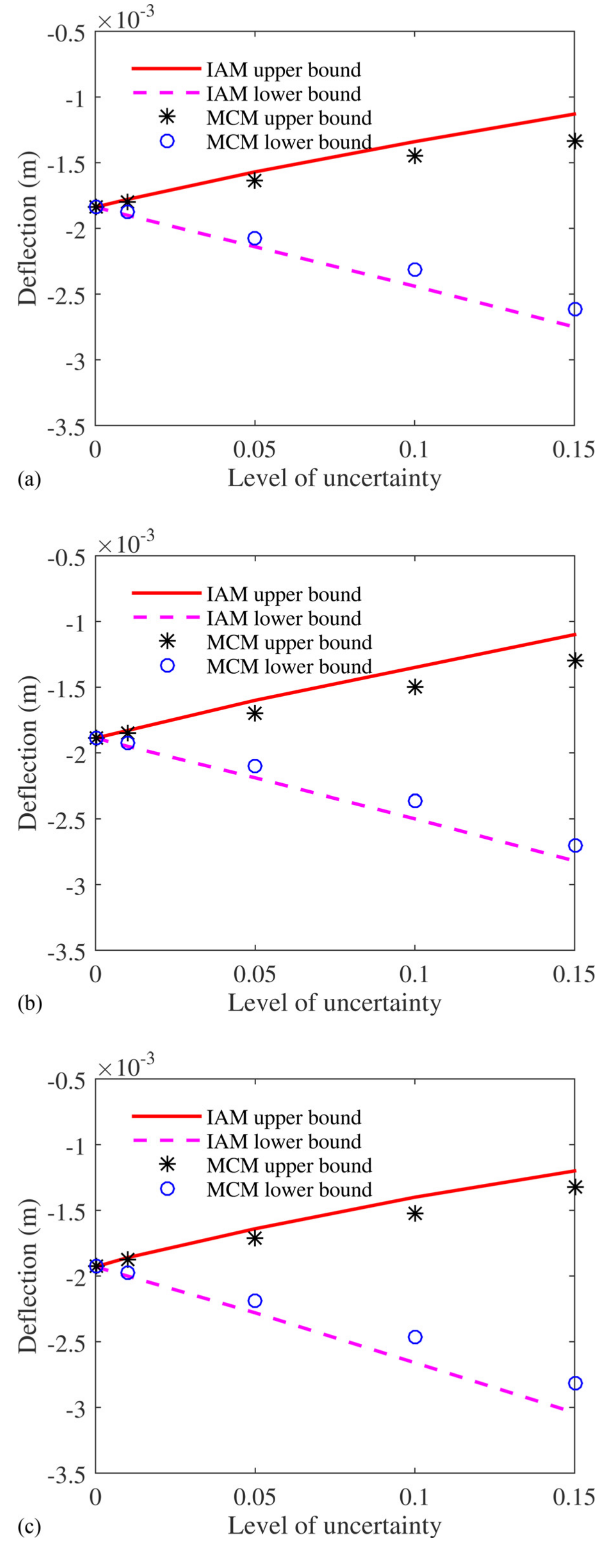

Fig. 10. Bounds of maximum deflection of Girder 4 at midspan with different vehicle speeds: (a) $v = 10$ m/s; (b) $v = 20$ m/s; (c) $v = 30$ m/s

good balance between the accuracy and the computational effort, it is desirable to select those parameters that have significant impacts on the bounds, instead of all parameters, to implement the subinterval technique and set a suitable number of subintervals for the parameters.

Numerical Example

To illustrate the proposed method, a typical two-lane simply-supported slab-on-girder concrete bridge, designed in accordance with the AASHTO specification (AASHTO 2002), was selected in the present study. The bridge consists of five identical AASHTO Type-III girders with a girder spacing of 2.13 m. It has a span length of 12.19 m, roadway width of 9.75 m, and bridge deck thickness of 0.2 m. Diaphragms are placed at both span ends and the midspan of the bridge. Each girder is divided into 18 beam elements in the longitudinal direction, and girders are connected by the transverse beams, which are used to model the bridge deck and diaphragms. The cross section of the bridge is shown in Fig. 6.

A 5-axle semitrailer truck, as shown in Fig. 2, was chosen as the vehicle model. To fully illustrate the IAM, a total of 27 parameters of the vehicle and bridge, all of which can affect the VBI behavior, were chosen as interval parameters. The midpoint values of these

Table 2. Relative Differences between Bounds of Deflection Obtained by IAM and MCM

		Upper bounds			Lower bounds		
Speed (m/s)	Level of uncertainty	IAM (mm)	MCM (mm)	Relative difference (%)	IAM (mm)	MCM (mm)	Relative difference (%)
10	0.01	–1.78	–1.80	1.11	–1.90	–1.88	–1.06
	0.05	–1.57	–1.63	3.68	–2.14	–2.08	–2.88
	0.10	–1.34	–1.45	7.59	–2.44	–2.31	–5.63
	0.15	–1.13 (–1.28)	–1.34	15.67 (4.48)	–2.75	–2.62	–4.96
20	0.01	–1.83	–1.85	1.08	–1.95	–1.93	–1.04
	0.05	–1.60	–1.70	5.88	–2.19	–2.10	–4.29
	0.10	–1.35 (–1.45)	–1.50	10.00 (3.33)	–2.50	–2.36	–5.93
	0.15	–1.10 (–1.28)	–1.30	15.38 (1.54)	–2.82	–2.70	–4.44
30	0.01	–1.86	–1.88	1.06	–2.00	–1.98	–1.01
	0.05	–1.64	–1.71	4.09	–2.28	–2.19	–4.11
	0.10	–1.40	–1.52	7.89	–2.66	–2.47	–7.69
	0.15	–1.20 (–1.27)	–1.32	9.09 (3.79)	–3.04	–2.82	–7.80

Note: The values in parentheses were calculated with the subinterval technique.

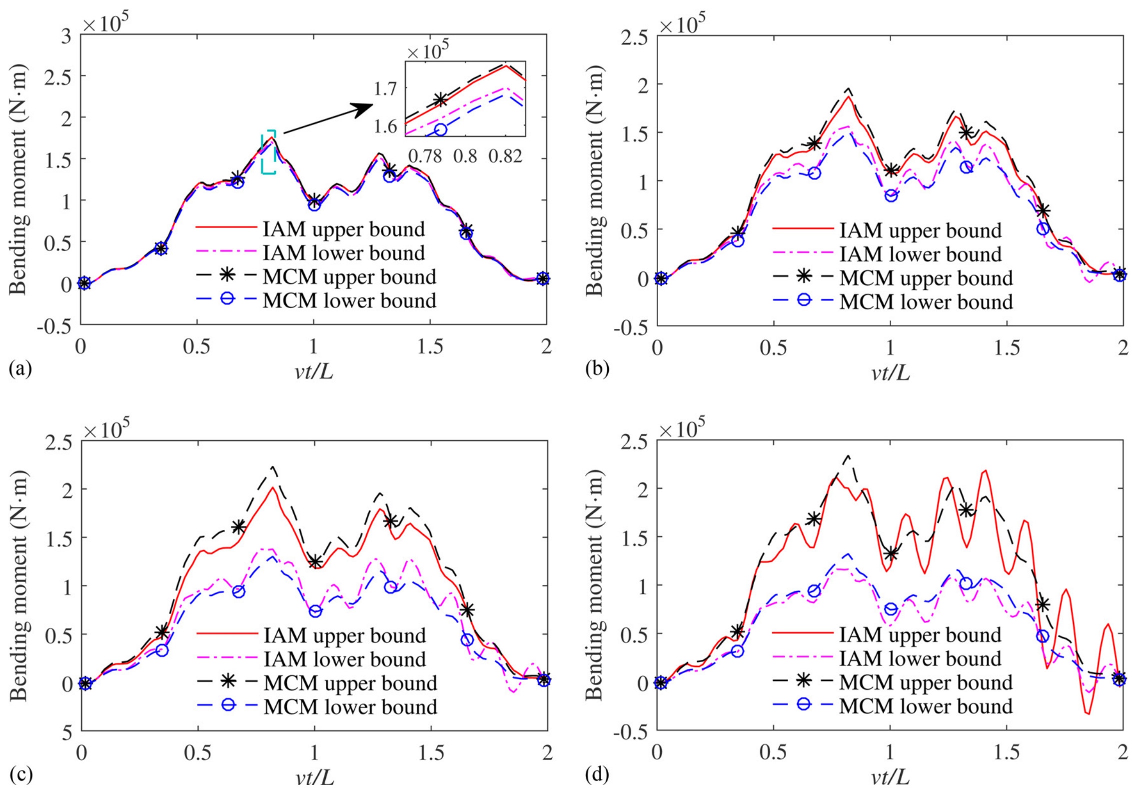

Fig. 11. Bounds of bending moment time histories at midspan of Girder 4 under different levels of uncertainty (vehicle speed = 20 m/s): (a) $\eta = 0.01$; (b) $\eta = 0.05$; (c) $\eta = 0.10$; (d) $\eta = 0.15$

parameters, which can be found in the literature (Harris et al. 2007; Huang et al. 1993; OBrien et al. 2010), are listed in Table 1. To simplify the analysis, a sensitivity analysis can usually be performed first to select those parameters that have more significant influence on the target response than the others. All interval parameters are assumed to have the same uncertainty level in the same case, whereas different uncertainty levels are studied in different cases.

The vehicle is assumed to cross the bridge along the right lane, as shown in Fig. 6. Under this loading condition, Girder 4 appears to bear the largest amount of load among all girders and was therefore selected in the following analysis. It should be noted that, because the road surface condition was found to have a negligible effect on the accuracy of the results, only the results of good-class road surface conditions are presented in this study for the sake of brevity.

To verify the effectiveness of the IAM, the MCM was also applied to obtain the lower and upper bounds of the bridge responses. To implement the Monte Carlo simulation, the uniform distribution was assumed over the interval of each parameter (Roy and Oberkampf 2011). A convergence test was performed on the MCM, and the results are shown in Fig. 7, where the vehicle speed is set to 20 m/s and the uncertainty level of the parameters is 0.10. Fig. 7 indicates that both the upper and lower bounds of both the bridge deflection and bending moment at the midspan of Girder 4 start converging at approximately 2,000 simulations. In addition, performing such large-scale dynamic simulation of the VBI analysis is very time-consuming because of the complexity of its time-dependent equation of motion, especially when the number of DOFs of the bridge structure is large and when a large volume of traffic flows needs to be considered (OBrien et al. 2010). Based on the convergence test results of the MCM, the bounds yielded by 2,000 Monte Carlo simulations are therefore taken as reference results when calculating the relative differences of the bounds predicted by the IAM and MCM.

Bounds of Bridge Deflection

The bounds of bridge deflection are solved by the PSO algorithm. The two acceleration coefficients in the algorithm are both set to 2, and the range of inertia weight is from 0.4 to 0.9 (Liu et al. 2013). Fig. 8 depicts the upper and lower bounds of the deflection time histories at the midspan of Girder 4 obtained by the IAM and 2,000 Monte Carlo simulations, respectively, under different uncertainty levels of the interval parameters. In all of these scenarios, the vehicle speed is set to 20 m/s. The results calculated by the IAM, especially the lower bounds, are in good agreement with those calculated by the MCM, even at large uncertainty levels, such as 0.10 and 0.15. More specifically, the upper bounds predicted by the IAM are larger than those predicted by the MCM, whereas the lower bounds predicted by the IAM are smaller than those predicted by the MCM. Therefore, the IAM can produce a slightly conservative estimation of the interval width of the bridge deflection.

In addition, because of the use of the first-order Taylor series expansion, the contribution of each interval parameter to the interval width of bridge deflection can be easily obtained by evaluating the magnitude of $\{[\partial d(x^c,t)]/\partial a_i^I\}\Delta a_i$ in Eq. (12), and the results are shown in Fig. 9. For the sake of brevity, only the first three parameters of the bridge or vehicle that have the biggest contributions to maximum bridge deflection are plotted. Fig. 9(a) shows that the Young's modulus of the girder (a_1) and bending moment of inertia of girder (a_{10}) play key roles in determining the bridge deflection, as expected. In addition, Fig. 9(b) shows that the factor that has the biggest contribution to bridge deflection among all 15 vehicle parameters selected is the tire stiffness (a_{23}). The reason is that the wheelbase length of the vehicle (12.10 m) is almost equal to the length of the bridge (12.19 m) in this example, thus the dynamic response of the bridge is sensitive to the characteristics of the single axle or wheel; in contrast, according to Eq. (6), the contribution of interval parameter a_i, $\{[\partial d(x^c,t)]/\partial a_i^I\}\Delta a_i$, can be rewritten as $\{[\partial d(x^c,t)]/\partial a_i^I\}a_i^c\eta_i$; therefore, the contribution of a_i is not only

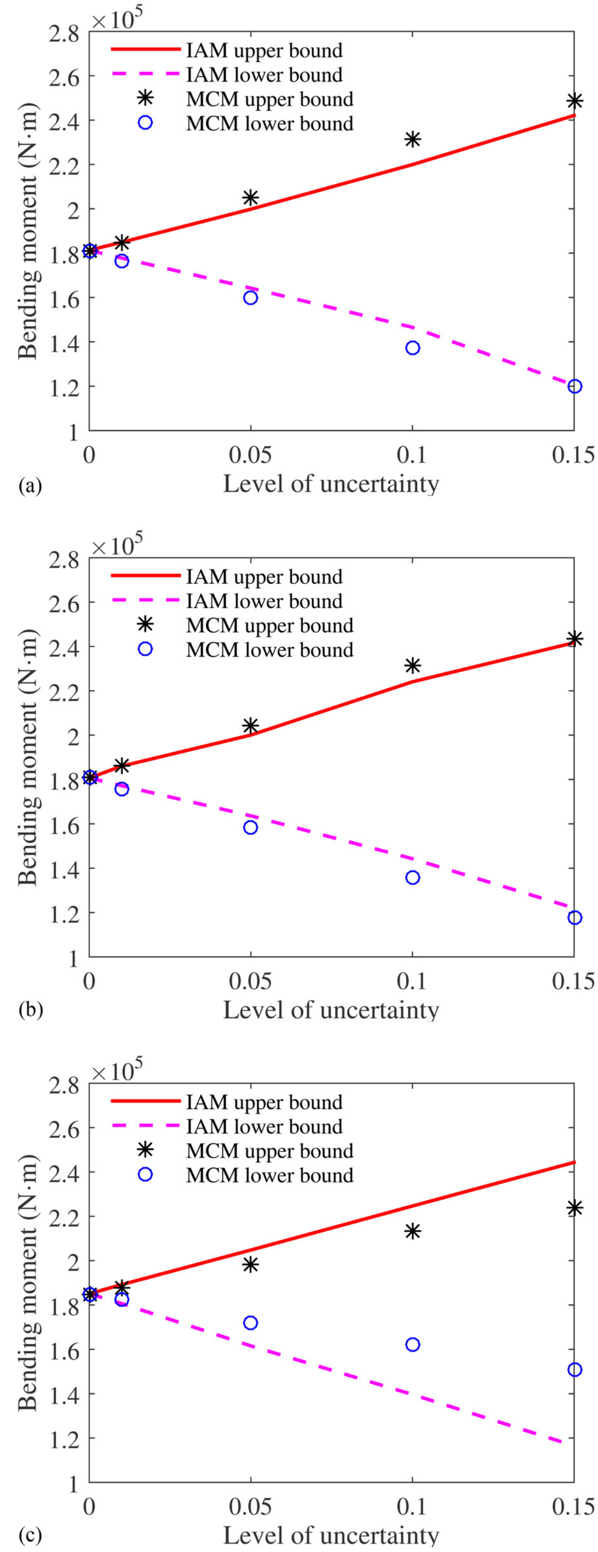

Fig. 12. Bounds of maximum bending moment of Girder 4 at midspan with different vehicle speeds: (a) $v = 10$ m/s; (b) $v = 20$ m/s; (c) $v = 30$ m/s

influenced by the sensitivity term $[\partial d(x^c, t)]/\partial a_i^I$, but also depends on the magnitude of $a_i^c \eta_i$. Given the assumption that all interval parameters have the same uncertainty level (η_i), those parameters possessing large midpoint values (a_i^c), such as tire stiffness, can greatly affect the interval width of the deflection. Fig. 9 also clearly shows that the increase of uncertainty level of input interval parameters of the VBI system can lead to the increase of the interval width of bridge deflection.

To further investigate the effectiveness of the IAM in the VBI analysis, several cases with different vehicle speeds under good road surface conditions were considered. For each specific case with a given vehicle speed, the VBI analysis was set to run 10 times with 10 sets of randomly generated road surface profiles under the good-class road surface condition for the sake of statistical significance (Deng and Cai 2010; Oliva et al. 2013), and the average value of the 10 independent results was obtained. The lower and upper bounds of the bridge maximum deflection at the midspan are plotted in Fig. 10, and the relative differences between the results calculated by the IAM and the MCM are listed in Table 2.

Fig. 10 clearly shows that the interval widths calculated by the IAM cover those determined by 2,000 Monte Carlo simulations. As shown in Table 2, the relative differences are generally less than 10%, whereas in a couple of cases, they reach over 15%. To demonstrate the effect of the subinterval technique in improving accuracy, four cases that have large differences were further refined by performing the subinterval technique. According to Fig. 9, the first three parameters of bridge and vehicle that significantly affect the bridge deflection are a_1, a_{10}, and a_{23}, respectively. Therefore, these parameters were selected to undergo the subinterval technique, where the original interval of each parameter is divided into two subintervals, indicating that a total of $2 \times 2 \times 2 = 8$ interval analyses need to be performed to obtain the final bounds. The updated bounds and relative differences are shown in the parentheses next to the original results in Table 2. The comparison between the original and updated results shows that the accuracy was greatly improved by adopting the subinterval technique.

Bounds of Bending Moment

Once the displacement responses are expressed by the first-order Taylor series, the task of determining the bounds of the bending moment at the midspan of Girder 4 is transformed into the optimization problem described in Eq. (15), which is also solved by the PSO algorithm. Fig. 11 depicts the bounds of the bending moment time histories at the midspan of Girder 4 obtained by the IAM and 2,000 Monte Carlo simulations, respectively. The lower and upper bounds calculated by the IAM agree well with those calculated by the MCM when the uncertainty level is less than 0.1, and the difference in the bounds obtained by the two methods tends to increase as the uncertainty level increases.

Fig. 12 and Table 3 show the upper and lower bounds of the maximum bending moment and the relative differences between the results calculated by the IAM and MCM, respectively. The subinterval technique was also used to improve the results of the cases with large relative differences. Again, Table 3 shows that the subinterval technique can greatly improve the accuracy of the results. With the subinterval technique, good accuracy can be achieved with the largest relative difference being controlled within 10%. However, it is noteworthy that the IAM no longer always yields conservative bounds like the case for bridge deflection. This is partly because neglecting the higher-order terms of the Taylor series in Eq. (7) may bring uncertainty to the results (Xia and Yu 2014). Meanwhile, the dependency phenomenon in Eq. (14) can also affect the interval width of the bounds of bending moment.

Computational Efficiency of the IAM

Table 4 shows the comparison of computing time required by the IAM, with or without use of the subinterval technique, versus MCM to achieve relatively stable bounds of the response of the VBI system. The simulations were carried out on a PC with a 3.5-GHz 6-core CPU and 64-GB RAM. It was found that the IAM is much more efficient than the MCM by significantly reducing the number of times needed to solve the VBI equation. Compared to the large number of times MCM needed to solve Eq. (2) to find the bounds of responses of the VBI system with satisfactory accuracy, the IAM only needed to solve Eq. (8) once to get the midpoint response and Eq. (9) 27 times to get the partial derivatives with respect to each interval parameter. When the subinterval technique is applied, the accuracy is greatly enhanced at the cost of increasing the computational time. However, the IAM with subinterval technique is still much more computationally efficient than the MCM.

Application of IAM to a Field Bridge Example

The IAM was also applied to a field bridge to verify whether it can successfully predict reasonable bounds of the responses of a field

Table 3. Relative Differences between Bounds of Bending Moment Obtained by IAM and MCM

		Upper bounds			Lower bounds		
Speed (m/s)	Level of uncertainty	IAM ($\times 10^5$ N m)	MCM ($\times 10^5$ N m)	Relative difference (%)	IAM ($\times 10^5$ N m)	MCM ($\times 10^5$ N m)	Relative difference (%)
10	0.01	1.85	1.85	0.00	1.78	1.76	1.14
	0.05	2.00	2.05	–2.44	1.64	1.60	2.50
	0.10	2.20	2.32	–5.17	1.47	1.37	7.30
	0.15	2.42	2.49	–2.81	1.20	1.20	0.00
20	0.01	1.86	1.86	0.00	1.77	1.76	0.57
	0.05	2.00	2.04	–1.96	1.64	1.58	3.80
	0.10	2.24	2.31	–3.03	1.44	1.36	5.88
	0.15	2.42	2.44	–0.82	1.22	1.18	3.39
30	0.01	1.89	1.88	0.53	1.81	1.82	–0.55
	0.05	2.05	1.99	3.02	1.62	1.72	–5.81
	0.10	2.25	2.13	5.63	1.40 (1.54)	1.62	–13.58 (–4.94)
	0.15	2.44 (2.37)	2.24	8.93 (5.80)	1.16 (1.38)	1.51	–23.18 (–8.61)

Note: The values in parentheses were calculated with the subinterval technique.

bridge under vehicle loads when only limited information about the bridge and vehicle is available. The tested bridge is located over Cypress Bayou in District 61 on LA 408 East, Baton Rouge, Louisiana. It has three simple spans, each measuring 16.764 m (55 ft) in length, and the third span of the bridge was instrumented. A dump truck with a single front axle and a 2-axle rear axle group was used in the test. Fig. 13 shows the profile of the tested bridge and the loading position of the truck. Deflections and bending strains at the bottom of the seven girders at the midspan were recorded when the truck crossed the bridge along Lane 1 at a speed of 17.88 m/s (40 mi/h). The roughness of the bridge deck was measured by a laser profile. More information about the test setup can be found in Deng and Cai (2009).

Table 4. Comparison of Computing Time between IAM and MCM

Method	Calculation times of VBI equation	Computing time (s)
IAM	28	1,500
IAM with subinterval technique	224	12,000
MCM (2,000 times)	2,000	110,000

The tested bridge was modeled by the grillage method. Each girder consists of 30 beam elements in the longitudinal direction, and the bridge deck and diaphragms were modeled by the transverse beams. The dump truck was represented by a full-scale 2-axle vehicle model with a total of 7 DOFs. The parameters of the tested bridge and truck are listed in Table 5 (Deng and Cai 2010).

Considering the possible uncertainties in the bridge and vehicle parameters resulting from the lack of sufficient data, several important parameters were chosen as interval parameters based on the sensitivity analysis in Fig. 9. For the bridge, the major factor

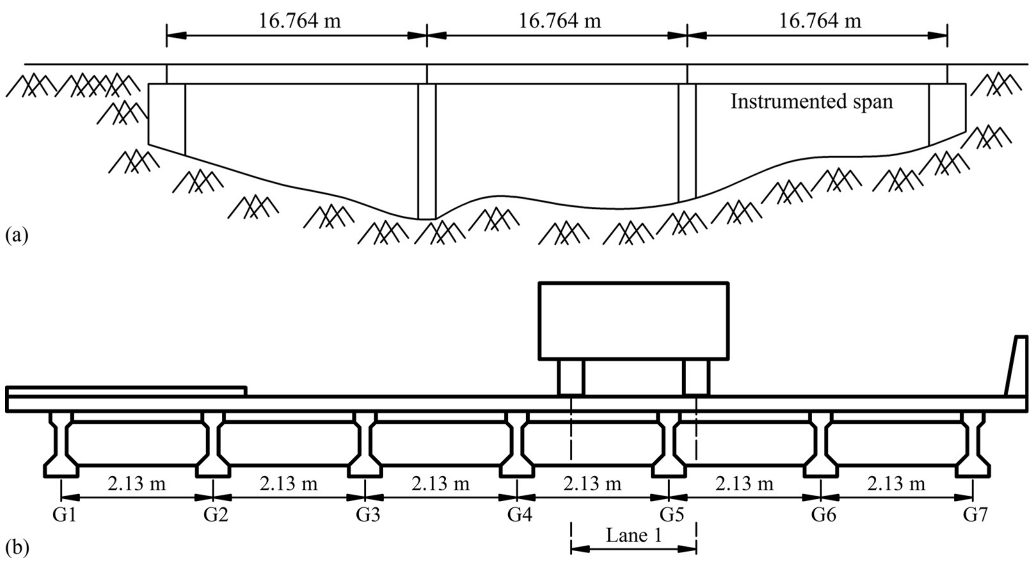

Fig. 13. Test setup: (a) profile of tested bridge; (b) cross section of bridge and loading position

Table 5. Parameters of Tested Bridge and Vehicle and Their Levels of Uncertainty

Parameter	Description of parameter	Value	Level of uncertainty	Reference
Bridge parameter	Young's modulus of the girders (Pa)	2.77×10^{10}	0.147	Tabsh and Nowak (1991)
	Young's modulus of the deck (Pa)	2.48×10^{10}	—	
	Young's modulus of the diaphragms (Pa)	1.00×10^{10}	—	
	Density of the deck (kg/m^3)	2.71×10^3	—	
	Density of the girders and diaphragms (kg/m^3)	2.40×10^3	—	
	Torsional moment of inertia of girders (m^4)	7.20×10^{-3}	—	
	Torsional moment of inertia of diaphragms (m^4)	6.06×10^{-3}	—	
	Bending moment of inertia of girders (m^4)	7.54×10^{-2}	—	
	Bending moment of inertia of diaphragms (m^4)	0.29×10^{-2}	—	
Vehicle parameter	Sprung mass (kg)	24,808	—	
	Pitching moment of inertia (kg·m^2)	172,160	—	
	Rolling moment of inertia (kg·m^2)	31,496	—	
	Axle mass (kg)	725.4	—	
	Steer suspension stiffness (N/m)	727,812	0.158	Harwood et al. (2003)
	Rear suspension stiffness (N/m)	1,969.034	0.236	Harwood et al. (2003)
	Steer suspension damping (N·s/m)	2,189.60	—	
	Rear suspension damping (N·s/m)	7,181.80	—	
	Front tire stiffness (N/m)	1,972,900	0.137	Fancher et al. (1986)
	Rear tire stiffness (N/m)	4,735,000	0.137	Fancher et al. (1986)

J. Bridge Eng., 2016, 21(9): 04016046

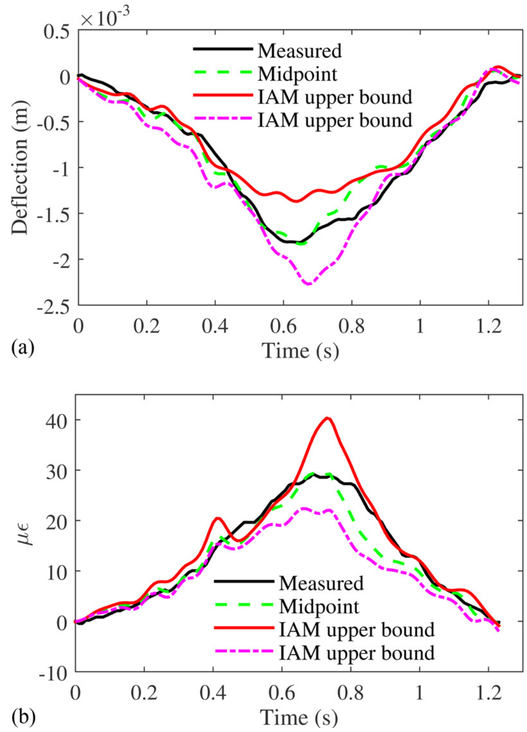

Fig. 14. Predicted bounds of responses of Girder 4 at midspan in the field testing example: (a) deflection time histories; (b) bending strain time histories

affecting the bridge responses is the bending stiffness (EI), which follows normal distribution and has a coefficient of variance (COV) of 0.075 (Tabsh and Nowak 1991). By adopting an interval that represents a 95% confidence level, an equivalent uncertainty level of 1.96 times the COV is used. For the purpose of simplifying the computation process, only Young's modulus (E) of the girders is treated as the interval parameter whereas the bending moment of inertia (I) is assumed to have a fixed value. For the vehicle, the weight can be easily measured, whereas the stiffness of the suspension systems and tires, which can influence bridge dynamic responses significantly, is often difficult to measure and is thus selected as the interval parameters here. The uncertainty levels of the selected interval parameters are determined based on the available information in the literature and are believed to be realistic to a certain extent.

The proposed IAM with the subinterval technique was then used to predict the bounds of the deflections and bending strains of the tested bridge with the existence of those nonprobabilistic uncertainties, and the results are plotted in Fig. 14. Fig. 14 shows that the predicted midpoint responses match the measured bridge responses very well, which proves that the VBI model can simulate the physical dynamic behavior of the bridge under vehicular load with good accuracy. Furthermore, the IAM predicts reasonable bounds of both bridge deflections and strains that contain the measured responses.

This example demonstrates that, when information about some key parameters is limited in the practice of bridge assessment, the proposed IAM can be utilized as a useful tool to estimate reasonable bounds of bridge responses by assuming reasonable uncertainty levels for the uncertain parameters based on the limited data available or experience. It should be noted that the degree to which the predicted bounds approach their true values still depends on the accuracy of the assumptions made on the uncertain parameters. However, as compared to the traditional probabilistic methods, the IAM does not need to know or assume the distribution types of the uncertain parameters and can predict reasonable bounds of responses with better accuracy based on limited information available.

Summary and Conclusions

In this paper, an interval analysis method for the dynamic analysis of a VBI system with nonprobabilistic uncertainties is proposed. This method can be applied to predicting the bounds of vehicle-induced bridge responses for complicated VBI systems for which no closed-form solutions are available, and the influence of the road roughness needs to be considered. In the proposed method, the responses of the VBI system are approximated by the first-order Taylor series, and the bounds of bridge responses can be explicitly given. To avoid the possible extreme overestimation induced by the direct interval arithmetic, the task of determining the bounds of the bridge responses is transformed into the optimization problem solved by the PSO algorithm. The subinterval technique is also adopted to further improve the accuracy of the results. The results from the numerical example show that both the bounds of bridge deflection and bending moment predicted by the IAM are in good agreement with those calculated by the MCM in most cases, even at large parameter uncertainty levels, while requiring much less computational effort.

The results from this study demonstrate that the IAM can be efficiently applied to predicting the extreme dynamic responses of complicated VBI systems with nonprobabilistic uncertainties without much sacrifice of accuracy as compared to the MCM. An example is also provided to illustrate the applicability of the IAM to the assessment of field bridges when the information about the bridge and vehicle parameters is limited. The results show that, under such circumstances, this method can provide reasonable bounds for the bridge responses of interest, which are very helpful in the decision-making process in practice, especially when the accuracy of the predicted responses is critical.

Acknowledgments

The authors acknowledge the financial support provided by the National Natural Science Foundation of China (Grant Nos. 51208189 and 51478176) and the Excellent Youth Foundation of Hunan Scientific Committee (Grant No. 14JJ1014).

References

AASHTO. (2002). *Standard specifications for highway bridges*, Washington, DC.

Au, F. T. K., Cheng, Y. S., and Cheung, Y. K. (2001). "Effects of random road surface roughness and long-term deflection of prestressed concrete girder and cable-stayed bridges on impact due to moving vehicles." *Comput. Struct.*, 79(8), 853–872.

Deng, L., and Cai, C. S. (2009). "Identification of parameters of vehicles moving on bridges." *Eng. Struct.*, 31(10), 2474–2485.

Deng, L., and Cai, C. S. (2010). "Development of dynamic impact factor for performance evaluation of existing multi-girder concrete bridges." *Eng. Struct.*, 32(1), 21–31.

Deng, L., Yu, Y., Zou, Q., and Cai, C. S. (2015). "State-of-the-art review of dynamic impact factors of highway bridges." *J. Bridge Eng.*, 10.1061/(ASCE)BE.1943-5592.0000672, 04014080.

Ding, L., Hao, H., and Zhu, X. Q. (2009). "Evaluation of dynamic vehicle axle loads on bridges with different surface conditions." *J. Sound Vib.*, 323(3–5), 826–848.

Dodds, C. J., and Robson, J. D. (1973). "The description of road surface roughness." *J. Sound Vib.*, 31(2), 175–183.

Fancher, P. S., Ervin, R. D., Winkler, C. B., and Gillespie, T. D. (1986). "A factbook of the mechanical properties of the components for single-unit and articulated heavy trucks. Phase I. Final report." *UMTRI-86-12*, Univ. of Michigan Transportation Research Institute, Ann Arbor, MI.

González, A., Rattigan, P., OBrien, E. J., and Caprani, C. (2008). "Determination of bridge lifetime dynamic amplification factor using finite element analysis of critical loading scenarios." *Eng. Struct.*, 30(9), 2330–2337.

Han, W., Wu, J., Cai, C. S., and Chen, S. (2015). "Characteristics and dynamic impact of overloaded extra heavy trucks on typical highway bridges." *J. Bridge Eng.*, 10.1061/(ASCE)BE.1943-5592.0000666, 05014011.

Harris, N. K., OBrien, E. J., and González, A. (2007). "Reduction of bridge dynamic amplification through adjustment of vehicle suspension damping." *J. Sound Vib.*, 302(3), 471–485.

Harwood, D. W., Torbic, D. J., Richard, K. R., Glauz, W. D., and Elefteriadou, L. (2003). "Review of truck characteristics as factors in roadway design." *NCHRP Rep. No. 505*, Transportation Research Board, Washington, DC.

Huang, D. Z., Wang, T. L., and Shahawy, M. (1993). "Impact studies of multigirder concrete bridges." *J. Struct. Eng.*, 10.1061/(ASCE)0733-9445(1993)119:8(2387), 2387–2402.

Liu, N., Gao, W., Song, C., Zhang, N., and Pi, Y.-L. (2013). "Interval dynamic response analysis of vehicle-bridge interaction system with uncertainty." *J. Sound Vib.*, 332(13), 3218–3231.

Ma, Y., Liang, Z., Chen, M., and Hong, J. (2013). "Interval analysis of rotor dynamic response with uncertain parameters." *J. Sound Vib.*, 332(16), 3869–3880.

Ma, Y., Wang, L., Zhang, J., Xiang, Y., Peng, T., and Liu, Y. (2014). "Hybrid uncertainty quantification for probabilistic corrosion damage prediction for aging RC bridges." *J. Mater. Civ. Eng.*, 10.1061/(ASCE)MT.1943-5533.0001096, 04014152.

Muhanna, R. L., and Mullen, R. L. (2001). "Uncertainty in mechanics problems—Interval-based approach." *J. Eng. Mech.*, 10.1061/(ASCE)0733-9399(2001)127:6(557), 557–566.

OBrien, E. J., Cantero, D., Enright, B., and González, A. (2010). "Characteristic dynamic increment for extreme traffic loading events on short and medium span highway bridges." *Eng. Struct.*, 32(12), 3827–3835.

Oliva, J., Goicolea, J. M., Antolín, P., and Astiz, M. Á. (2013). "Relevance of a complete road surface description in vehicle–bridge interaction dynamics." *Eng. Struct.*, 56, 466–476.

Roy, C. J., and Oberkampf, W. L. (2011). "A comprehensive framework for verification, validation, and uncertainty quantification in scientific computing." *Comput. Methods Appl. Mech. Eng.*, 200(25–28), 2131–2144.

Sankararaman, S., and Mahadevan, S. (2011). "Likelihood-based representation of epistemic uncertainty due to sparse point data and/or interval data." *Reliab. Eng. Syst. Saf.*, 96(7), 814–824.

Tabsh, S., and Nowak, A. (1991). "Reliability of highway girder bridges." *J. Struct. Eng.*, 10.1061/(ASCE)0733-9445(1991)117:8(2372), 2372–2388.

Wu, J., Luo, Z., Zhang, N., and Zhang, Y. (2015). "A new uncertain analysis method and its application in vehicle dynamics." *Mech. Syst. Sig. Process.*, 50–51, 659–675.

Xia, B., and Yu, D. (2012). "Modified sub-interval perturbation finite element method for 2D acoustic field prediction with large uncertain-but-bounded parameters." *J. Sound Vib.*, 331(16), 3774–3790.

Xia, B., and Yu, D. (2014). "Modified interval and subinterval perturbation methods for the static response analysis of structures with interval parameters." *J. Struct. Eng.*, 10.1061/(ASCE)ST.1943-541X.0000936, 04013113.

Zhang, H., Mullen, R. L., and Muhanna, R. L. (2010). "Interval Monte Carlo methods for structural reliability." *Struct. Saf.*, 32(3), 183–190.